

Limit Analysis of Stability of Circular Foundation Pit

Cui Xinzhuang, Yao Zhanyong, Jin Qing, Wu Shimei

School of Civil Engineering

Shandong University

School of Civil Engineering, South Campus of Shandong University, Jingshi Road 73#, Jinan, 250061
China

cuixz@sdu.edu.cn zhanyong-y@sdu.edu.cn jinqing@sdu.edu.cn wsm@mail.sdu.edu.cn

<http://www.sdu.edu.cn>

Abstract: - Circular foundation pits often appear in civil engineering. In order to obtain the critical depth of the non-supported circular foundation pit, the upper-bound method in plasticity mechanics was employed. The assumed slip surface in analysis was the rotational logspiral surface. The kinematically admissible velocity field was obtained according to the associated flow rule for Coulomb material, and the optimization model of the critical depth was established and solved with SQP optimization algorithm. The variations of the critical depth with the slope angle, the ratio of depth to radius of pit and the internal friction angle of soil were studied. The arch effect of the circular foundation pit makes the critical depth larger than the critical height of the plane slope; however, when the ratio of depth to radius of pit approaches zero, the upper-bound solution of the former approaches that of the latter. If the ratio of depth to diameter of pit is less than 10, the arch effect may be ignored and the foundation pit can be analyzed as the plane slope with the method of slices. Comparisons between upper-bound solution(*UBS*), the solution from approximate slip line theory(*SLS*) and finite difference solution(*FDS*) showed that *UBS* is less than *SLS* and larger slightly than *FDS*.

Key-Words: - circular foundation pit; slope; critical depth; limit analysis; upper-bound method; arch effect

1 Introduction

Limit analysis theory is an important branch of plastic mechanics. It was developed from the metal plastic theory and has already been extended to rock and soil mechanics now. Limit analysis was used to solve some engineering problems, such as slope stability and limit load[1-8]. It contains two kinds of basic methods, i.e. the upper-bound method and the lower-bound method. Based on upper-bound theorem, the upper-bound method needs to establish the kinematically admissible failure mechanism and velocity field in advance. The velocity field must meet motion boundary conditions and associated plastic flow rule. Based on lower-bound theorem, the lower-bound method needs to set up statically admissible stress field which must satisfy equilibrium equation, stress boundary condition and not disobey the failure criterion which is Mohr-Coulomb failure criterion for rock and soil.

Limit analysis can give the definite bounds of some problems such as the slope critical height and the pile bearing capacity[1-8]. However, the solution from rigid limit equilibrium method, which is another analysis method used extensively in

geomechanics, is difficult to tell that it is an upper-bound solution or lower-bound solution.

For Some failure mechanisms used in limit equilibrium method, the corresponding kinematically admissible velocity fields for limit analysis can be obtained according to virtual work principle. So the limit equilibrium solutions from these failure mechanisms are upper-bound solutions, just as the Sarma method which is an important method solving the safety factor of slope. But for Some failure mechanisms used frequently in limit equilibrium method, the corresponding kinematically admissible velocity field can't be set up, so the limit equilibrium solutions aren't upper-bound solutions, just as the vertical slices method and the circular slide method used for the stability analysis of slope. For vertical slices method, interslice force can't satisfy Mohr-Coulomb failure criterion. For Coulomb material obeying associated flow rule, the angle between velocity jump vector and the tangent of the slip surface should be equal to the internal friction angle of material, but for the circular rigid slide mechanism, we can't set up any velocity field satisfying this.

In addition, the limit equilibrium solutions can't be used as the lower-bound solution because the stress field in rigid body is not known.

The upper-bound method is applied more extensively than the lower-bound method because the establishment of statically admissible stress field is rather difficult. While solving the problem with the upper-bound method, a valid failure mechanism is assumed firstly, and then the internal energy dissipation rate and the work done by external loads are calculated respectively and equated with each other. Thus a serial of upper-bound solutions corresponding to the specific mechanism are obtained, and finally, the optimum upper-bound solution can be gotten by employing optimization technology[8]. Donald I and Chen Z Y studied the stabilities of plan strain and three-dimension slopes using rigid blocks translational failure mechanism[1-2]. Murff obtained the lateral bearing capacity of pile with three-dimensional deforming mechanism[3]. However, limit analysis hasn't be used to solve the axisymetrical problem as yet. Axisymetrical problems appear frequently in geotechnical engineering such as the stabilities of circular foundation pit and most in-situ tests such as CPT and SPT. The aim of this paper is to solve the non-supported critical depth of the circular foundation pit to demonstrate the application of upper-bound method to axisymetrical problem. The circular foundation pit is often analyzed as the plane strain problem when the ratio of depth to radius of pit is large enough. When the ratio of depth to radius of pit is small, however, the plane strain solution is not accurate because the arch effect of soil mass largely enhances the stability of the pit.

In this paper, limit analysis method will be employed to solve the critical depth of the circular foundation pit. Based on the work of Березанцев В Г[9], limit equilibrium solution was also obtained and compared with upper-bound solution. In analysis, soil is assumed homogeneous and isotropic, and the failure is axisymetrical.

2 Problem Formulation

2.1 Upper-bound Theorem

When a slope sliding mass above a potential slip surface is in a plastic limit state (Fig.1), and when any kinematically admissible velocity field is introduced to the sliding mass, based on upper-bound theorem, the energy dissipation within the

sliding mass and along the slip surface is less than the work rate done by the external loads.

$$\int_{\Omega} \sigma_{ij} \dot{\epsilon}_{ij}^* d\Omega + \int_{\Gamma} \sigma_r \dot{\epsilon}_r^* d\Gamma \leq \mathbf{WV}^* + \mathbf{TV}^* \quad (1)$$

where σ_{ij} and σ_r denote a set of stresses within the sliding mass region Ω and on a potential slip surface Γ in a plastic limit state. $\dot{\epsilon}_{ij}^*$, $\dot{\epsilon}_r^*$ and \mathbf{V}^* denote a set of kinematically admissible strain rates within the sliding mass, on the potential slip surface Γ and the velocity field of the mass, respectively. \mathbf{W} and \mathbf{T} are the weight of sliding mass and the external forces acting on the sliding mass, respectively.

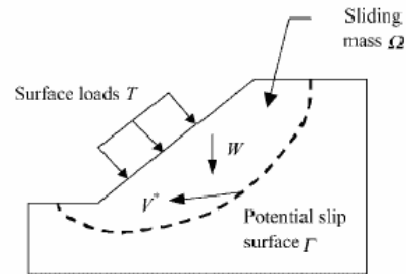


Fig.1 Sliding mass of slope

2.2 Failure Mechanism

As a kind of slope, the common failure surface of circular foundation pit is logspiral surface, just as shown in fig.2. The rotating center of failure face is on the axis of foundation pit. The function of logspiral surface is:

$$r = r_0 e^{(\theta - \theta_0) \tan \phi} \quad (2)$$

Where ϕ is internal friction angle of soil, r_0 is polar radius of point b where $\theta = \theta_0$.

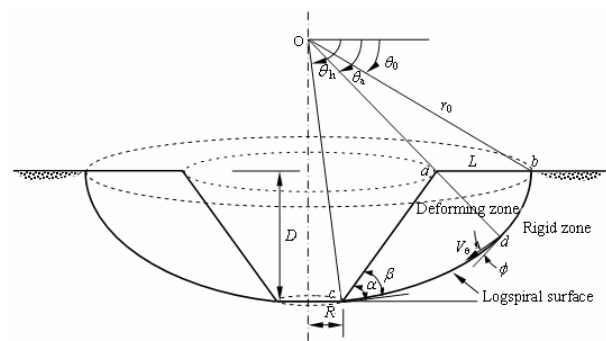


Fig.2 Failure mechanism of circular foundation pit

The shape of foundation pit can be described with the ratio of depth to bottom radius D/R and slope angle α of foundation pit, as shown in fig.2. Once they are known, the dimension of the whole failure zone can be determined by two independent variables: the characteristic angle θ_0 and the depth of foundation pit D .

In Fig.2, L is the length of ab ; β is defined as split angle that is the angle between slip surface and pit wall at slope toe. Let $A = D/r_0$ and $B = L/r_0$. Then equations (3)-(5) can be derived from Fig.1:

$$A = \sin \theta_h \cdot e^{(\theta_h - \theta_0) \tan \phi} - \sin \theta_0 \quad (3)$$

$$B = \cos \theta_0 - \cos \theta_h \cdot e^{(\theta_h - \theta_0) \tan \phi} - A \cdot \cot \alpha \quad (4)$$

$$\beta = \theta_h - \phi + \alpha - \pi / 2 \quad (5)$$

The function of the line ab is:

$$r = \frac{\sin \theta_0}{\sin \theta} r_0 \quad (6)$$

The function of the line ac is:

$$r = \frac{\sin \theta_0 + \tan \alpha \cdot (\cos \theta_0 - B)}{\sin \theta + \tan \alpha \cdot \cos \theta} r_0 \quad (7)$$

The polar angle of the point a is:

$$\theta_a = \arccot \frac{\cos \theta_0 - B}{\sin \theta_0} \quad (8)$$

According to geometrical relationship, θ_h can be obtained from the following equation:

$$\frac{D}{R} = \frac{\sin \theta_h e^{(\theta_h - \theta_0) \tan \phi} \cos \theta_h}{\sin \theta_h e^{(\theta_h - \theta_0) \tan \phi} - \sin \theta_0} \quad (9)$$

2.3 Velocity Field

V_r , V_θ and V_ψ are radial, tangential and circumferential velocity components in spherical coordinate system (r, θ, ψ) , respectively. According to the associated plastic flow rule, $V_r = V_\psi = 0$ on the logspiral failure surface. Here we assume further that $V_r = V_\psi = 0$ in the whole deforming region. V_θ can be determined according to the associated plastic flow rule. In spherical coordinates, tensor- strain-rates are written as:

$$\left. \begin{aligned} \dot{\epsilon}_r &= 0 \\ \dot{\epsilon}_\theta &= \frac{1}{r} \frac{\partial V_\theta}{\partial \theta} \\ \dot{\epsilon}_\psi &= \frac{\cot \theta}{r} V_\theta \\ \dot{\gamma}_{r\theta} &= \frac{1}{2} \left(\frac{\partial V_\theta}{\partial r} - \frac{V_\theta}{r} \right) \\ \dot{\gamma}_{r\psi} &= 0 \\ \dot{\gamma}_{\theta\psi} &= 0 \end{aligned} \right\} \quad (10)$$

Because $\dot{\gamma}_{r\psi} = \dot{\gamma}_{\theta\psi} = 0$, $\dot{\epsilon}_\psi$ is principal strain rate. According to the normality of $\dot{\epsilon}_r$, $\dot{\epsilon}_\theta$ and $\dot{\epsilon}_\psi$, we know $\dot{\epsilon}_r$ and $\dot{\epsilon}_\theta$ are also principal strain rates. Subsequently we can know:

$$\dot{\gamma}_{r\theta} = \frac{1}{2} \left(\frac{\partial V_\theta}{\partial r} - \frac{V_\theta}{r} \right) = 0 \quad (11)$$

For Coulomb material matching associated flow rule, Chen W F gave the following equation[8]:

$$T \cdot \sum \dot{\epsilon}_t + \sum \dot{\epsilon}_c = 0 \quad (12)$$

where $T = \tan^2(\frac{\pi}{4} - \frac{\phi}{2})$, $\sum \dot{\epsilon}_t$ and $\sum \dot{\epsilon}_c$ are the summation of principal tensional strain rates and the summation of principal compressive strain rates, respectively. Note that tensional strain rates are positive in this paper.

If $\phi = 0$, the following equation can be obtained from Eq.(12):

$$\sum \dot{\epsilon}_t + \sum \dot{\epsilon}_c = 0 \quad (13)$$

Eq.(13) reflects the incompressibility of Tresca material and it's suited for undrained case of saturated soil mass.

Because $\dot{\epsilon}_r = 0$, we know from equation (12) that there is a maximum strain rate $\dot{\epsilon}_{\max}$ and a minimum strain rate $\dot{\epsilon}_{\min}$ in $\dot{\epsilon}_\theta$ and $\dot{\epsilon}_\psi$. In order to obtain velocity field, we studied the following two cases.

$$(1) \quad \dot{\epsilon}_\psi = \dot{\epsilon}_{\max}, \dot{\epsilon}_\theta = \dot{\epsilon}_{\min}$$

From Eq.(10) and Eq.(12), we obtain:

$$T \cot \theta V_\theta + \frac{\partial V_\theta}{\partial \theta} = 0 \quad (12)$$

From Eq.(11) and Eq.(12), we obtain:

$$T \cdot r \cot \theta \frac{\partial V_\theta}{\partial r} + \frac{\partial V_\theta}{\partial \theta} = 0 \quad (13)$$

The partial differential equations above can be solved using the variable separation method. Let $V_\theta = f(\theta) \cdot g(r)$, and substitute it into Eq.(13) and obtain:

$$\frac{rf'(r)}{f(r)} = -\frac{g'(\theta) \tan \theta}{g(\theta) T} = C_1 \quad (14)$$

where C_1 is a constant.

Solving the two ordinary differential equations in Eq.(14), $f(r)$ and $g(\theta)$ can be obtained. The final expression of V_θ is:

$$V_\theta = f(r)g(\theta) = Cr^{C_1} \sin^{-TC_1} \theta \quad (15)$$

where C is a constant.

Substituting Eq.(15) into Eq.(11) or Eq.(12) leads to $C_1 = 1$, thus Eq.(15) can be written as

$$V_\theta = Cr \sin^{-T} \theta \quad (16)$$

Because $\dot{\epsilon}_\psi = \dot{\epsilon}_{\max} > 0$, we can know $C > 0$ after substituting Eq.(16) into Eq.(10). At the same

time, $0 < \theta < \frac{\pi}{2}$. So we can know $V_\theta > 0$. This indicates that soil mass slides down and doesn't disobey the true physical case.

$$(2) \quad \dot{\epsilon}_\theta = \dot{\epsilon}_{\max}, \dot{\epsilon}_\psi = \dot{\epsilon}_{\min}$$

Using the same methods, we obtain:

$$V_\theta = Cr \sin^{-\frac{1}{T}} \theta \quad (17)$$

Because $\dot{\epsilon}_\psi = \dot{\epsilon}_{\min} < 0$, $C < 0$ can be known after substituting Eq.(17) into Eq.(10). At the same time, $0 < \theta < \frac{\pi}{2}$. So we can know $V_\theta < 0$. This implies that soil mass slides up and disobeys the true physical condition.

Now we know that the maximum and minimum principal strain rate are $\dot{\epsilon}_\psi$ and $\dot{\epsilon}_\theta$, respectively, and V_θ is determined uniquely by Eq. (16).

2.4 Internal Energy Dissipation Rate and External Force Work Rate

Energy dissipation occurs on the slip surface and in the deforming zones. Here work is done by gravity of soil only because there are no other external forces.

2.4.1 Energy Dissipation Rate

The internal energy dissipation rates include those on failure surface and in plasticity deforming zone. According to the literature [8], the energy dissipation rate of unit area on failure surface is calculated with the following equation:

$$\dot{E}_1 = cV_s \quad (18)$$

where c is cohesion of soil; V_s is tangential velocity jump across the failure surface.

The total energy dissipation rate \dot{D}_1 on failure surface is obtained by integrating Eq.(18) along the surface that is gotten by rotating the logspiral line bc about the axes of foundation pit, as shown in Fig.2:

$$\dot{D}_1 = \int_{\theta_0}^{\theta_h} 2\pi r_{bc}^2 \cos \theta / \cot \theta \dot{E}_1 d\theta \quad (19)$$

where r_{bc} is obtained by Eq.(2).

Literature [8] also gave the expression of the internal energy dissipation rate of unit volume in plasticity deforming zone:

$$\dot{E}_2 = 2c\sqrt{T} \sum \dot{\epsilon}_i \quad (20)$$

Once velocity field is known, strain rate field can be obtained according to geometric equations. But it's difficult to obtain the analytic expression of principal strain rates and this limits the application of Eq.(20).

In orthogonal coordinates system $\{x, y, z\}$, if $\{V_x, V_y, V_z\}$ of deforming region is known, the plastic normal strain rate field $\{\dot{\epsilon}_x, \dot{\epsilon}_y, \dot{\epsilon}_z\}$ can be obtained according to geometry equations. For orthogonal coordinates system, there is:

$$\begin{aligned} \dot{\epsilon}_V &= \dot{\epsilon}_x + \dot{\epsilon}_y + \dot{\epsilon}_z = \dot{\epsilon}_1 + \dot{\epsilon}_2 + \dot{\epsilon}_3 \\ &= \sum \dot{\epsilon}_t + \sum \dot{\epsilon}_c \end{aligned} \quad (21)$$

where $\dot{\epsilon}_i (i=1,2,3)$ are principal plastic strain rates, $\dot{\epsilon}_V$ is the bulk strain rate, $\sum \dot{\epsilon}_t$ and $\sum \dot{\epsilon}_c$ are as shown in Eq.(12).

From Eq.(12) and Eq.(21), $\sum \dot{\epsilon}_t$ and $\sum \dot{\epsilon}_c$ can be obtained:

$$\sum \dot{\epsilon}_t = \frac{\dot{\epsilon}_V}{1-T} \quad (22)$$

$$\sum \dot{\epsilon}_c = \frac{\dot{\epsilon}_V}{1-1/T} \quad (23)$$

From Eq.(20) and Eq.(22), a new expression of the energy dissipation rate per unit volume can be obtained:

$$\dot{E} = c \cot \phi \dot{\epsilon}_V \quad (24)$$

Eq.(24) implies that the energy dissipation rate per unit volume can be expressed with the function of plastic bulk strain rate. In Eq.(24), $c \cot \phi$ is the coordinate of vertex of the right hexagonal pyramid whose surface represents Mohr-Coulomb yield surface in principal stress space. When $\phi \rightarrow 0$, Coulomb material will tend to Tresca material, $c \cot \phi \rightarrow \infty$ and $\dot{\epsilon}_V \rightarrow 0$.

For Tresca material, the internal energy dissipation rate per unit volume is:

$$\dot{E}_2 = 2c|\dot{\epsilon}|_{\max} \quad (25)$$

Comparing Eq.(24) with Eq.(25), the following equation can be obtained:

$$\lim_{\phi \rightarrow 0} \cot \phi \dot{\epsilon}_V = 2|\dot{\epsilon}|_{\max} \quad (26)$$

Because the plastic bulk strain rate can be obtained directly from velocity field and geometry equations, Eq.(24) provides a general solving method of the energy dissipation rate per unit volume. The method simplifies the solving process of the energy dissipation rate.

The energy dissipation rate of unit volume in deforming region of circular pit can be obtained from Eq.(10) and Eq.(24):

$$\dot{E}_2 = Cc(1-T) \cot \phi \cot \theta \sin^{-T} \theta \quad (27)$$

The total internal energy dissipation rate in deforming region \dot{D}_2 can be calculated by integrating Eq.(27) in the annular domain that is obtained by rotating the area abc about the axes of foundation pit, as shown in Fig.2:

$$\begin{aligned} \dot{D}_2 &= \int_{\theta_0}^{\theta_a} \int_{r_{ab}}^{r_{bd}} 2\pi r^2 \cos \theta \dot{E}_2 d\theta dr \\ &+ \int_{\theta_h}^{\theta_c} \int_{r_{ac}}^{r_{cd}} 2\pi r^2 \cos \theta \dot{E}_2 d\theta dr \end{aligned} \quad (29)$$

where r_{ab} and r_{ac} are obtained by Eq.(6) and Eq.(7), respectively, r_{bd} and r_{cd} are obtained by Eq.(2).

2.4.2 External Force Work Rate

For the foundation pit studied in this paper, the gravity of soil is the only external force. The gravity work rate of unit volume soil is expressed:

$$\dot{w} = \gamma \mathcal{W}_\theta \cos \theta \quad (30)$$

where γ is soil bulk density.

The total gravity work rate of soil mass \dot{W} can be obtained by integrating Eq.(30) in the annular

domain that is obtained by rotating the area abc about the axes of foundation pit, as shown in Fig.2:

$$\dot{W} = \int_{\theta_0}^{\theta_a} \int_{r_{ab}}^{r_{bd}} 2\pi r^2 \cos \theta \omega d\theta dr + \int_{\theta_a}^{\theta_h} \int_{r_{ac}}^{r_{cd}} 2\pi r^2 \cos \theta \omega d\theta dr \quad (31)$$

where r_{ab} and r_{ac} are obtained by Eq.(6) and Eq.(7), respectively, r_{bd} and r_{cd} are obtained by Eq.(2).

The integrations above have no analytic solution, so we need to employ numerical methods to solve them.

2.5 Mathematic Model

According to upper-bound theorem, there is

$$\dot{D}_1 + \dot{D}_2 = \dot{W} \quad (32)$$

The critical depth of foundation pit can be expressed as:

$$D_{cr} = \frac{c}{\gamma} f(\theta_0) \quad (33)$$

In order to obtain the minimum upper-bound solution of critical depth, we need to solve the minimum of function $f(\theta_0)$. Let $N_s = \min f(\theta_0)$, where N_s is a dimensionless variable, independent of c and γ and only related to ϕ , α and D/R . The mathematic model used to solve the minimum upper-bound solution of critical depth of foundation pit is as follows:

$$N_s = \min f(\theta_0) \left\{ \begin{array}{l} B \geq 0 \end{array} \right\} \quad (34)$$

The constraint condition in Eq.(34) makes sure that point b is on the right of point a , as shown in Fig.2.

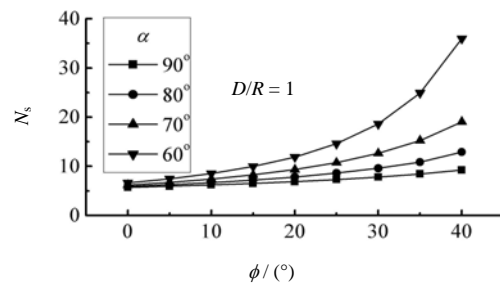
Base on SQP optimization algorithm, we used matlab software to solve the minimum upper-bound of critical depth of circular foundation pit.

3 Results and Analysis

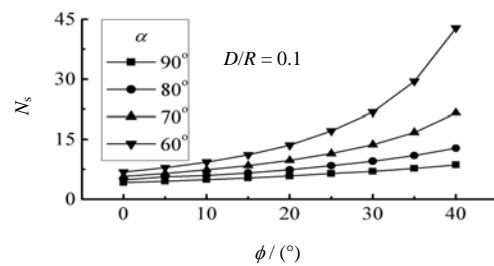
3.1 Critical Height

When D/R is equal to 0.1 and 1.0, respectively, the variations of N_s with ϕ and α are showed in Fig.3. N_s increases with the increment of ϕ . Moreover, the bigger ϕ is, the more rapidly N_s varies. N_s decreases with the increment of α , furthermore, the smaller α is, the more rapidly N_s varies.

Fig.4 shows variations of N_s with D/R and ϕ when $\alpha = 90^\circ$. N_s increases with the increment of D/R . Moreover, when D/R is very small, the variation of N_s is also small. This shows that the arch effect of soil mass largely enhances the stability of the foundation pit.



(a) $D/R = 1$



(b) $D/R = 0.1$

Fig.3 Varying curves of N_s with ϕ and α

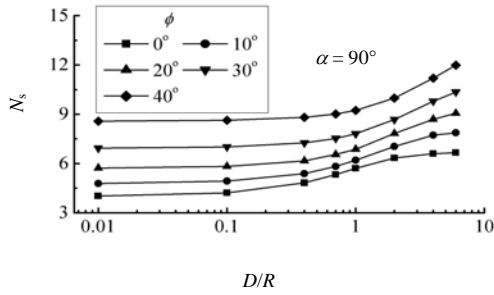


Fig.4 Varying curves of N_s with D/R and ϕ

Fig.5 shows variations of characteristic angle θ_0 with ϕ and α . θ_0 increases with the increments of ϕ and α . Once θ_0 and N_s are known, other characteristic angles θ_a and θ_h and characteristic dimensions such as r_0 , L and so on can all be obtained. Thus the location and shape of the slip surface can be decided.

When D/R is very small, the circular foundation pit can be analyzed as the plane slope. In limit analysis of plane slope, two kinds of failure mechanisms are usually used, i.e. rigid blocks translational and rotational mechanisms, as shown in fig.6 and fig.7, respectively. In table 1, N_s of vertical circular foundation pit with $D/R = 0.001$ and vertical plane slope from different failure mechanisms are given, respectively. When D/R is very small, it can be found that N_s of circular foundation pit approximates that of plan slope from rigid blocks translational mechanism, and both of them are slightly greater than that from rigid blocks rotational mechanism.

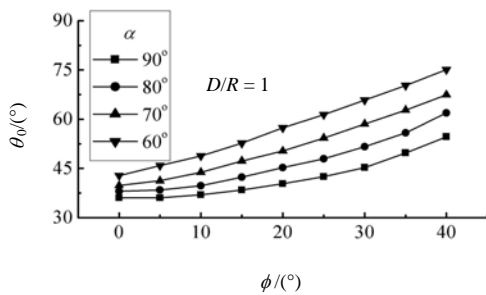


Fig.5 Varying curves of θ_0 with ϕ and α

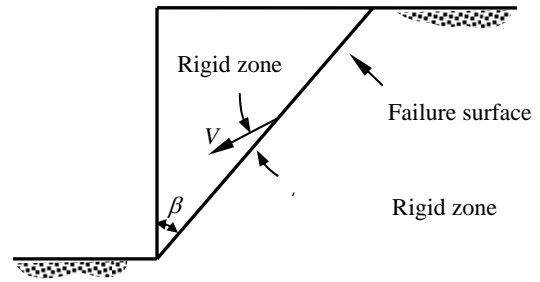


Fig.6 Rigid blocks translational failure mechanism

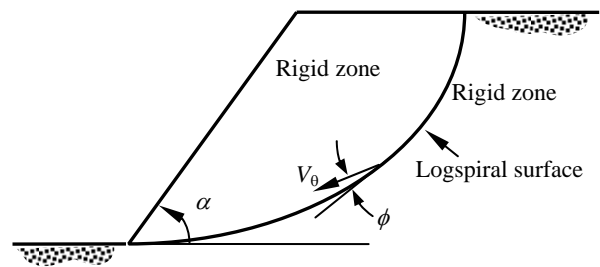


Fig.7 Rigid blocks rotational failure mechanism

According to the results computed with the method proposed in this paper, we also know that $\theta_0 \rightarrow \theta_h$ when $D/R \rightarrow 0$. This implies that the rotational logspiral surface degenerates to the circular truncated surface. At the same time, the critical slip angle β_{cr} corresponding to D_{cr} is the same as the critical value of β shown in Fig.5 and both are equal to $(\pi/4 - \phi/2)$. But this doesn't imply that the plasticity deforming region degenerates to rigid region because internal energy dissipation rate expressed by Eq.(24) isn't equal to zero.

Table 1 N_s obtained from some failure mechanisms

ϕ	N_s		
	Plane slope with rigid blocks translational failure mechanism	Plane slope with rigid blocks rotational failure mechanism	Circular foundation pit of $D/R=0.001$ with axisymmetrical failure mechanism
0°	4.000	3.8300	4.0021
10°	4.7666	4.5925	4.7685
20°	5.7115	5.5116	5.7229
30°	6.9261	6.6935	6.9289
40°	8.5741	8.3330	8.5785

The stability of plane slope often is analyzed with vertical slices method, e.g. Janbu method. For plan slope, when $\phi = 20^\circ$, N_s from Janbu method is equal to 6.01. It is very similar to the upper limit solution of circular foundation pit whose D/R is 0.2. So the arch effect of the foundation pit may be ignored and it can be regarded as plan slope and analyzed with the slices method when the ratio of depth to diameter of pit is less than 10.

3.2 Slip Surfaces

Knowing θ_0 and θ_h , the shape and location of slip surface can be obtained. Here, assume that d and h are the horizontal and vertical distance of any point on slip surface from foundation pit wall toe, just as point c shown in Fig.2. In order to plot slip surfaces from different cases on a diagram, normalize d and h with D_{cr} and obtain dimensionless variables d/D_{cr} and h/D_{cr} , respectively.

Fig.8 shows the effect of D/R on slip surface of cylindrical foundation pit when $\phi = 20^\circ$. With the increase of D/R , slip surface shrink inward.

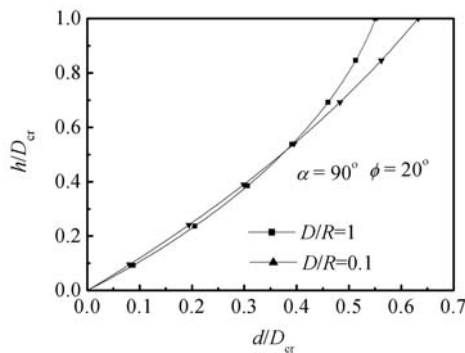


Fig.8 Effect of D/R on slip surface

Fig.9 shows the effect of ϕ on slip surface of cylindrical foundation pit when $D/R = 0.8$. With the increase of ϕ , slip surface shrink inward.

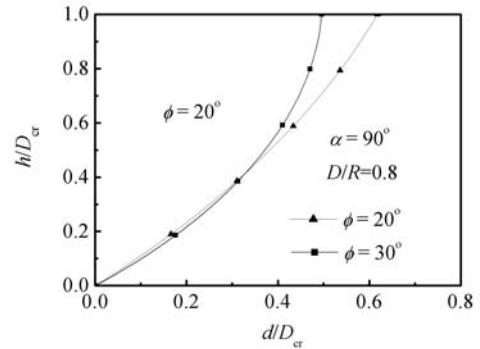


Fig.9 Effect of ϕ on slip surface

4 Discussions

The solution from slip-line theory (SLS) and the solution from finite difference method (FDS) were computed to be compared with the upper-bound solution (UBS).

4.1 Comparison of UBS with SLS

Using axisymmetrical slip-line theory, Везезанцев В Г obtained the approximate active earth pressure on retaining wall of cylindrical foundation pit [9], as shown in the following equation:

$$p_a = \gamma R \frac{\sqrt{T}}{\lambda - 1} \left[1 - \left(\frac{R}{Z} \right)^{\lambda - 1} \right] + c \cot \phi \left(\frac{R}{Z} \right)^\lambda T \quad (35)$$

where γ is soil bulk density, ϕ and c are internal friction angle and cohesion of soil, respectively, R is radius of cylindrical pit, $T = \tan^2 \left(\frac{\pi}{4} - \frac{\phi}{2} \right)$,

$\lambda = 2 \tan \phi / \sqrt{T}$, $Z = R + z\sqrt{T}$ and z is the depth under ground, as shown in Fig.10.

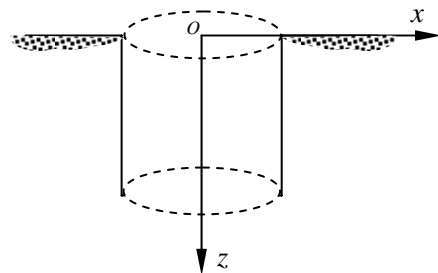


Fig.10 Cylindrical foundation pit

Let $R \rightarrow \infty$, we can obtain:

$$p_a = \gamma z T - 2c\sqrt{T} \quad (36)$$

From Eq.(36), the expression of active earth pressure is seen to be the same as Rankin formula for plane problem when R is very large.

In order to solve the critical depth of cylindrical foundation pit, following transaction method of Terzaghi and peck[10], the active earth pressure is intergrated along the depth and equating the integral zero:

$$\int_0^{D_{cr}} p_a dz = 0 \quad (37)$$

From Eq.(35) and Eq.(37), we can obtain:

$$\begin{aligned} & (A - B)(\lambda - 2)(\lambda - 1)\sqrt{T}D_{cr} \\ & - [BT(2 - \lambda) + A(\lambda - 1)]R \\ & + [BT(2 - \lambda)R + A(\lambda - 1)(\sqrt{T}D_{cr} + R)] \\ & \times \left(\frac{R}{\sqrt{T}D_{cr} + R}\right)^{\lambda-1} = 0 \end{aligned} \quad (38)$$

where $A = \gamma R \frac{\sqrt{T}}{\lambda - 1}$, $B = c \cot \phi$.

SLS of critical depth of cylindrical foundation pit can be obtained by solving Eq.(38) with numerical method.

Comparison was made between UBS and SLS, as shown in Fig.7. For cylindrical foundation pit, it can be seen that UBS is slightly greater than SLS when $\phi = 0$, however, in other cases, the former is always less than the latter.

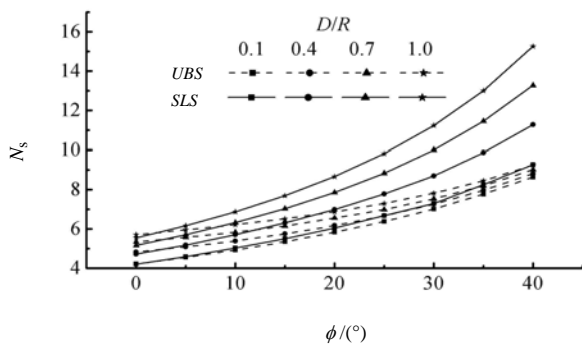


Fig.11 Comparison between UBS and SLS of critical depth

Assuming that N_{s1} and N_{s2} are UBS and SLS of N_s , respectively, the relation of N_{s1} and N_{s2} can be established. For cylindrical foundation pit,

$$D_{cr} = f(c, \gamma, R, \phi) \quad (39)$$

Normalize two sides of Eq.(39) and we can obtain:

$$N_{s2} = \frac{D_{cr}\gamma}{c} = g\left(\frac{R\gamma}{c}, \phi\right) \quad (40)$$

From Eq.(33) and Eq.(34), we know

$$\frac{R\gamma}{c} = \frac{N_{s1}}{D/R} \quad (41)$$

From Eq.(40) and Eq.(41), we can obtain

$$N_{s2} = g\left(\frac{N_{s1}}{D/R}, \phi\right) \quad (42)$$

Eq.(42) gives the relation between N_{s1} and N_{s2} . For $D/R = 0.1 \sim 1.0$, the relation between N_{s1} and N_{s2} is

$$\left. \begin{aligned} N_{s2} &= 3.569 + 0.465e^t \\ t &= 0.517 + 5.642 \frac{D/R}{N_{s1}} + 0.052\phi \end{aligned} \right\} \quad (43)$$

Fig.12 shows the fitting effective of Eq.(43). The relation between N_{s1} and N_{s2} can be expressed well with Eq.(43).

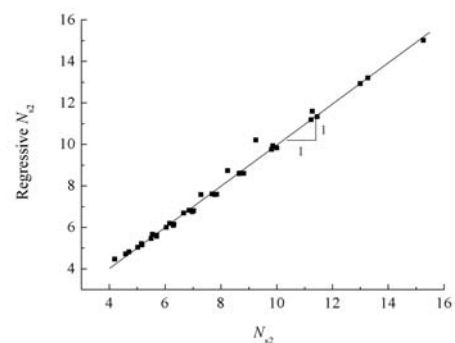


Fig.12 Fitting effective diagram

4.2 Comparison of UBS with FDS

FLAC/SLOPE program was used to compute the numerical solution of N_s . This program is a mini-version of FLAC(Fast Lagrangian Analysis of Continua) that is provided by Itasca Consulting Group, Inc. FLAC/Slope is designed specifically to perform factor-of-safety calculations for slope stability analysis. Besides two-dimensional plane-strain analysis, axisymmetric analysis can also be performed with FLAC/Slope.

FLAC/Slope provides an alternative to traditional limit equilibrium programs to determine factor of safety. Limit equilibrium codes use an approximate scheme - typically based on the method of slices -in which a number of assumptions are made (e.g., the location and angle of interslice forces). Several assumed failure surfaces are tested, and the one giving the lowest factor of safety is chosen. Equilibrium is only satisfied on an idealized set of surfaces. In contrast, FLAC/Slope provides a full solution of the coupled stress/displacement, equilibrium and constitutive equations, just as FEM[11-13]. Given a set of properties, the system is determined to be stable or unstable. By automatically performing a series of simulations while changing the strength properties (shear strength reduction technique), the factor of safety can be found to correspond to the point of stability, and the critical failure surface can be located.

According to strength reduction technique, strength parameters used in stability analysis can be written as:

$$c' = \frac{c}{F_s}, \quad \tan \phi' = \frac{\tan \phi}{F_s} \quad (44)$$

where F_s is safety factor, c' and ϕ' are mobile cohesion and mobile internal friction angle of soil, respectively.

When critical failure happens under c' and ϕ' , F_s can be obtained from Eq.(44). In order to obtain the critical depth of cylindrical pit, change the depth gradually and obtain the corresponding safety factor. When the safety factor is approximately 1.0, the depth is the critical one. Fig.13 illustrates the computing process in which safety factor varies with depth. In Fig.13, $\gamma = 20 \text{ kN/m}^3$, $c = 10 \text{ kPa}$, $\phi = 30^\circ$ and $R = 2.5 \text{ m}$.

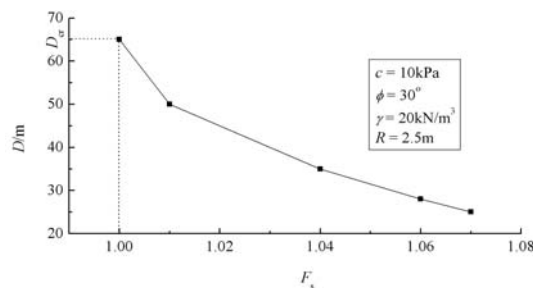


Fig.13 $D-F_s$ curve

From Eq.(33) and Eq.(34), we obtain

$$N_s = \frac{D_{cr}\gamma}{c} \quad (45)$$

Some numerical results of critical depth of cylindrical pit were listed in table 2 and compared with UBS. It can be seen that UBS of N_s is larger slightly than FDS.

Table 2 Comparison of UBS with FDS

ϕ	D/R	N_s	
		FDS	UBS
	26.00	130.0	134.1
30°	1.00	30.0	35.2
	0	6.5	6.7
	4.08	20.4	28.7
20°	0.35	10.4	11.9
	0	5.4	5.51
	5.40	10.8	12.4
10°	0.21	6.2	7.1
	0	4.3	4.6

Failure surface can be obtained along with D_{cr} . For the case of $\gamma = 20 \text{ kN/m}^3$, $c = 10 \text{ kPa}$, $\phi = 20^\circ$ and $R = 2.5 \text{ m}$, the failure of pit is illustrated in Fig.14. The failure surface is seen to approach the rotational logspiral surface assumed in limit analysis in this paper.

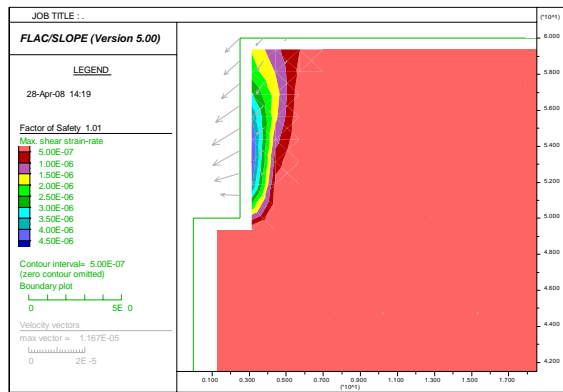


Fig.14 Failure surface

5 Conclusion

Assuming that soil mass is homogeneous and isotropic and the failure model of circular foundation pit is axisymmetrical, kinematically admissible failure mechanism and velocity field were established according to associated plastic flow rule. Using them, the stability of the circular foundation pit was analyzed and the limit upper-bound solution of critical height was obtained. The following are some important conclusions:

- (1) Critical depth increases with the decrement of slope angle of foundation pit and the increment of the ratio of depth to radius and internal friction angle of soil.
- (2) The arch effect of circular foundation pit makes its critical depth greater than the critical height of plane slope. However, the arch effect is unobvious when the ratio of depth to diameter of pit is less than 10.
- (3) When the ratio of depth to radius is very small, the upper-bound solution of circular foundation pit is very close to the one of plane slope obtained from rigid blocks translational failure mechanism. Moreover, on the axisymmetrical surface, the rotational logspiral failure line degenerates to straight line, and the critical slip angle is the same as plane slope from rigid blocks translational mechanism, however, the plasticity deforming zone isn't rigid yet.
- (4) UPS of the critical depth is less than SLS and larger slightly than FDS .

In this paper, the critical depth of the non-supported circular foundation pit was studied; however, further researches are urgent on the stability of circular pit reinforced, for example, by soil nails.

6 Acknowledgements

This work was supported by Chinses Natural Science Foundation(No.50708056) and Natural Science Foundation of Shandong Province, China(No. Q2006F02).

References:

- [1] Donald I, Chen Z Y. Slope stability analysis by the upper-bound approach: fundamentals and methods. *Canadian Geotechnical Journal*, Vol.34, No.6, 1997, pp. 853-862
- [2] Chen Z Y, Wang X G, Haberfield C, et al. A three-dimensional slope stability analysis method using the upper-bound theorem –Part 1: theory and methods. *International Journal of Rock Mechanics and Mining Sciences*, Vol.38, No.6, 2001, pp. 369-378
- [3] Murff J D, Hamilton J M. P-ultimate for undrained analysis of laterally loaded piles. *Journal of Geotechnical Engineering*, Vol.119, No.1, 1993, pp.91-107
- [4] Drescher A, Detourany E. Limit load in translational failure mechanism for associative non-associative materials. *Geotechnique*, Vol.43, No.3, 1993, pp.443-456
- [5] Otani J, Ochiai H and Yamamoto K. Bearing capacity analysis of reinforced foundation on cohesive soil. *Geotextiles and Geomembranes*, Vol.16, 1998, pp.195-206
- [6] Zheng X, Booker J R, Carter J P. Limit analysis of the bearing capacity of fissured materials. *International Journal of Solids and Structures*, Vol.37, 2000, pp.1211-1243
- [7] Porbaha A, Zhao A, Kobayashi M and Kishida T. Upper bound estimate of scaled reinforced soil retaining walls. *Geotextiles and Geomembranes*, Vol.18, 2000, pp.403-413
- [8] Chen W F. *Limit analysis and soil plasticity*. Amsterdam, the Netherlands: Elsevier Publishing Co., 1975
- [9] Везанцев В Г. *Axial-symmetrical limit equilibrium problems of loose media*. Beijing: China Architecture and Building Press, 1981
- [10] Terzaghi K, Peck R B. *Soil Mechanics in Engineering Practice*[M]. New York: Wiley, 1967
- [11] Lina V, Saulius V, Antanas S. Adaptive Finite Element Analysis for Solution of Complex Engineering Problems. *Wseas Transactions on Applied and Theoretical Mechanics*, Vol.1, 2006, pp.33-38
- [12] Barbieri A, Cecchi A. Analysis of masonry columns by a 3D FEM homogenisation procedure. *Wseas Transactions on Applied and Theoretical Mechanics*, Vol.2, 2006, pp.42-51

- [13] Dubravka M. On dimensional reduction in multiscale, finite element and atomistic analysis in solid mechanics. *Wseas Transactions on Applied and Theoretical Mechanics*, Vol.1, 2006, pp.16-24